# Charged-particle dynamics and interaction with Alfvén waves in fusion plasmas

Mariana Martins
mariana.martins@tecnico.ulisboa.pt
Instituto Superior Técnico, Lisbon, Portugal

June 2019

**Abstract**

For future fusion reactors, such as ITER, the study of the interaction between $\alpha$-particles and Alfvén Eigenmodes (AEs) is very important. In order to compute the trajectory of charged particles in the electromagnetic field of a tokamak, two approaches are considered: the full-orbit (FO) and the guiding-centre (GC) approximation. The integration of the equations of motion for the FO approach is accomplished and compared with two methods: the Boris algorithm and a fourth-order Runge-Kutta (RK4) method. When computing the full-orbit of charged particles in an equilibrium field, the Boris algorithm conserves better the energy and it is faster than RK4, making it the most suitable method for the task. The interaction between AEs and $\alpha$-particles is investigated and the orbits and the energy exchange computed with the GC and FO approaches are compared. First, the $\alpha$-particle that interacts resonantly with a mode with n=30 is studied. The orbits computed with GC and FO are in agreement, however the same is not observed for the energy exchange. Some corrections are tested to the energy exchange computed with GC which decreases the difference. Using a mode with n=12, several resonant particles are considered and GC and FO results are compared. The orbits of passing-particles agree well, but the agreement of the energy exchange is dependent on the value of $\rho_L k_\perp$. Using trapped particles, the orbits do not agree. In conclusion, FO computed with the Boris algorithm should be used when following particles that do not verify $\rho_L k_\perp \ll 1$ and for trapped particles.
**Keywords:** Nuclear fusion, Alfvén waves, Full-orbit, Guiding-centre

## 1. Introduction

The search for a clean and sustainable source of energy that can satisfy society's increasing requirements is a problem that scientists have been trying to solve for the last decades. Harnessing the energy from nuclear fusion reactions would be a safe, environmentally friendly source of energy with sufficient fuel reserves that could satisfy the high demand for energy in a sustainable way.

Due to its higher cross section at a lower temperature, the easier reaction to initiate is the fusion of two hydrogen isotopes, deuterium (${}^2_1D$) and tritium (${}^3_1T$), producing an $\alpha$-particle and a neutron [1]:

$$ {}^2_1D + {}^3_1T \rightarrow \alpha(3.5\ \text{MeV}) + n(14.1\text{MeV}). \qquad (1) $$

The controlled nuclear fusion reactions must occur in a confining device, in which, due to the high temperatures required, the matter is ionized in a state that is called a plasma. One of the configurations under study is the tokamak, a torus-shaped device that uses magnetic fields to confine the charged particles of the plasma. In this type of machine, external coils are used to produce a large toroidal magnetic field, $B_\phi$, and a toroidal current produces a smaller poloidal magnetic field, $B_\theta$, resulting in a helical field that wraps around the torus. The geometry of a tokamak is represented in figure 1, where $R_0$ is the major radius, $a$ the minor radius, $\theta$ the poloidal angle, $\phi$ the toroidal angle and $r$ the radial coordinate measured in the poloidal plane.

The International Thermonuclear Experimental Reactor (ITER) [2] is an international project to build the largest tokamak to date. This project aims to demonstrate the scientific and technological feasibility of nuclear fusion as an energy source. With ITER, it will be possible to investigate the physics of burning plasmas, where deuterium-tritium (D-T) fusion reactions produce neutrons and $\alpha$ particles that provide the desired energy and keep the plasma hot.

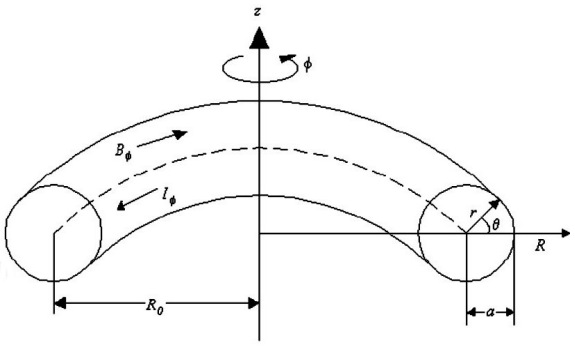


Figure 1: Diagram of a tokamak's geometry.

To reach the temperature necessary for fusion reactions, external heating mechanisms such as Neutral Beam Injection (NBI) and Ion Cyclotron Resonance Heating (ICRH) are used [3]. But the main goal is to reach ignition, when the fusion-born $\alpha$-particles become the main heating source of the plasma, by transferring energy to the other particles through collisions.

One of the key issues in sustainable nuclear fusion is the confinement of fast particles, with energies much higher than those of the bulk plasma. Fast particles include ions generated by external heating systems, such as NBI and ICRH, and fusion-born $\alpha$-particles [3]. This kind of particles is important since they heat up the plasma, thus allowing fusion reactions to happen. Therefore they should

be kept confined in the core in order to keep the plasma hot and also to prevent damages to the reactor's walls.

The confinement should be achieved through the imposed magnetic field. However, a problem arises in projected fusion devices, like the case of ITER [4], because the velocity of fusion-born $\alpha$-particles is close to the Alfvén speed, the phase speed of Alfvén waves. Due to their velocity, the $3.5MeV$ $\alpha$-particles may, by a resonant exchange of energy, drive unstable some Alfvén waves and perturb the background magnetic field that is used for confinement. The interplay between $\alpha$-particles and Alfvén waves may lead to a redistribution of the particles and eventually cause their transport away from the burning core. This transport can lead to losses and even stop fusion reactions since these particles no longer heat the plasma and it should be avoided. To minimize losses and increase power gain in future fusion reactors, it is important to understand which modes are more likely to be unstable and their impact on particle transport in different burning scenarios. With that in mind, there have been several reports on the stability of AEs in the 15 MA ITER baseline scenario [4, 5, 6, 7, 8]. These studies have found that Toroidal Alfvén Eigenmodes with $n \approx 30$ located at $r/a \approx 0.4$ are expected to be the most unstable modes in this scenario. These modes reach amplitudes of $\delta B/B \sim 10^{-4}$ and are not expected to lead to significant losses of $\alpha$-particles.

At a lowest-order approach, particle-tracer simulations can be used to understand the interplay between energetic particles and Alfvén waves. In these simulations, the particles' trajectories are followed in an equilibrium magnetic field upon which a perturbation, representing an Alfvén wave, is added allowing one to observe its influence on the particles' dynamics.

The trajectory of a charged particle in a uniform magnetic field consists of a rapid gyration around the field lines and a motion along the field lines, which results in a helical path [1]. If the order of magnitude of the gyroradius is much smaller than that of the spatial variation of the magnetic field and the gyrofrequency is much larger than the frequency of variation of the magnetic field, the rapid gyration can be ignored and the trajectory correspondent to the instantaneous centre of that gyration can be computed as an approximation to the actual particle's trajectory. This approximation is frequently used in particle-tracer simulations because it requires less computational efforts than computing the full-orbit of the charged particle. However, despite its computational efficiency, following the guiding-centre is not always accurate. When dealing with the equilibrium magnetic fields of tokamaks, the spatial variation of the field is usually much larger than the gyroradius of the plasma particles, therefore the guiding-centre approximation holds. But, when the magnetic field is perturbed, the spatial scale of its variation may be of the same order of the gyroradius and the approximation might not be valid anymore. In this case, the guiding-centre should not be used and a full orbit study must be performed.

Particle-following simulations which include the computation of the full-orbit have been done using codes such as ASCOT [9], SPIRAL [10], LOCUST [11] and JOREK-3D [12], among others. With these codes, full-orbit simulations have been proven to be necessary in several cases when the validity of the guiding-centre approximation is questionable and more accurate results are needed. The preferred integration method used for the full-orbit simulations is usually a volume-preserving algorithm, the Boris algorithm. For the guiding-centre simulations, a Runge-Kutta method is typically used.

In this work, a Runge-Kutta method and the Boris algorithm are compared to decide which one is the most adequate in full-orbit simulations. Then, full-orbit and guiding-centre simulations are performed to study the interaction between $\alpha$-particles and Alfvén Eigenmodes in order to understand when does the guiding-centre approximation fails and a full-orbit is necessary.

## 2. Alfvén waves

In a homogeneous plasma with a uniform magnetic field, shear Alfvén waves propagate along the magnetic field lines following the dispersion relation $\omega^2 = k_\parallel^2 v_A^2$. But in tokamaks, where the plasma is inhomogeneous and the magnetic field and the density are not uniform, this dispersion relation becomes more complex. Considering high aspect ratio tokamaks, i.e. $\frac{R_0}{a} \gg 1$, $k_\parallel$ can be approximated by [13]

$$k_\parallel \approx \frac{1}{R}\left(n - \frac{m}{q}\right), \tag{2}$$

where $n$ and $m$ are the toroidal and poloidal mode numbers, respectively, and $q$ is the safety factor that typically depends on a radial coordinate $r$. Therefore the dispersion relation also depends on $r$ and can be approximated by

$$\omega^2(r) \approx \omega_A^2\left(n - \frac{m}{q(r)}\right)^2 \tag{3}$$

with $\omega_A = \frac{v_A}{R}$ the Alfvén frequency. Waves that follow this dispersion relation form the Alfvén *continuum* [13]. These waves are characterized by having a different phase velocity for each radius, which makes very difficult for a perturbation to propagate in the plasma.

For the same toroidal mode number $n$, there are different branches of the dispersion relation (3) that are expected to cross each other, i.e., there are waves with the same frequency at the same location. However, in toroidal geometry, this degeneracy is resolved at that location, leading to the appearance of gaps in the Alfvén *continuum*.

Particles with velocities close to the Alfvén speed may excite Alfvén Eigenmodes (AEs) in these gaps, which may not be sufficiently damped by the *continuum* or other damping mechanisms. If excited, AEs may lead to a growing perturbation of the magnetic field that can affect particle confinement. The most likely AEs to be excited are the Toroidicity-Induced Alfvén Eigenmodes (TAEs) [13, 14], which are a coupling between modes with the same toroidal mode number, $\Delta n = 0$, but differ by one unit in the poloidal mode number, $\Delta m = 1$. For these AEs, the squared frequency $\omega^2$ matches for the two modes at a given radial location $r_{TAE}$, which directly leads to the following relation for TAEs [4]:

$$nq(r_{TAE}) - m = \frac{1}{2}. \tag{4}$$

## 3. Charged particle motion

The Lagrangian for a charged particle, with charge $z$ and mass $m$, in an electromagnetic field is

$$\mathcal{L} = \frac{1}{2} m g_{ki} \dot{q}^i \dot{q}^k - z\Phi + z\dot{q}^k A_k. \tag{5}$$

where $g_{ki}$ is the metric tensor, $q^k$ and $\dot{q}^k$ are the contravariant components of the particle's position and velocity, $\Phi$ is the electric potential and $A_k$ are the covariant components of the vector potential. To obtain the equations of motion, it is necessary to apply the Euler-Lagrange(E-L) equations

$$\frac{d}{dt}\left(\frac{\partial \mathcal{L}}{\partial \dot{q}^i}\right) = \frac{\partial \mathcal{L}}{\partial q^i} \tag{6}$$

and take into account that the electric field is $\mathbf{E} = -\nabla\Phi - \frac{\partial \mathbf{A}}{\partial t}$ and the magnetic field is $\mathbf{B} = \nabla \times \mathbf{A}$, giving

$$\ddot{q}^k + g^{ik}\Gamma_{ijn}\dot{q}^j\dot{q}^n = \frac{z}{m}(E^k + [\dot{\mathbf{q}} \times \mathbf{B}]^k). \tag{7}$$

where $\Gamma_{ijk}$ is the Christoffel symbol of the first kind defined as

$$\Gamma_{ijk} = \frac{1}{2}\left(\frac{\partial g_{ik}}{\partial q^j} + \frac{\partial g_{ij}}{\partial q^k} - \frac{\partial g_{jk}}{\partial q^i}\right). \tag{8}$$

These equations can be used to compute the trajectories of a charged particle in an electromagnetic field using any coordinate system. If a cartesian coordinate system is used, the Christoffel symbol is zero and the equations of motion become simply

$$m\frac{d\mathbf{v}}{dt} = z(\mathbf{E} + \mathbf{v} \times \mathbf{B}) \tag{9}$$

where $\dot{\mathbf{q}}$ was replaced by $\mathbf{v}$ as the particle velocity. This is the well-known equation of a charged particle in an electromagnetic field associated with the Lorentz force [1]. Although equation (9) is a lot simpler than (7), it can only be used when all quantities are defined in cartesian coordinates. If one wants to solve the equations of motion in a different coordinate system, equation (9) is inappropriate and (7) must be used instead.

### 3.1. Guiding-centre theory

The motion of a charged particle in a magnetic field can be split into two components: a motion in the magnetic field direction and a gyration around the magnetic field lines characterized by the cyclotron frequency $\Omega = \frac{zB}{m}$ and the Larmor radius $\rho_L = \frac{v_\perp}{\Omega} = \frac{mv_\perp}{zB}$. This motion is represented in figure 2. The fast gyrating component of the motion can be ignored if, within one gyration of the particle, the magnetic field is almost constant in time and uniform in space. This means that the conditions

$$\rho_L \nabla B \ll B, \quad \frac{1}{\Omega}\frac{\partial B}{\partial t} \ll B. \tag{10}$$

need to be verified. These expressions mean that the Larmor radius should be much smaller than the spatial variation of the magnetic field and that the cyclotron frequency should be much larger than any frequency of interest. Under these conditions, the motion of the particle can be described only by its guiding-centre. Defining $\mathbf{x}$ as the particle's position and $\mathbf{X}$ as the guiding-centre's position, the two are related by:

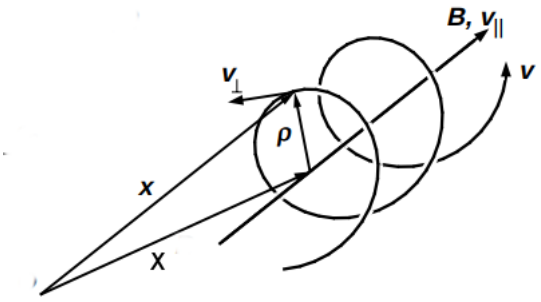


Figure 2: Diagram of a charged particle motion in a homogeneous magnetic field.

$$\mathbf{x} = \mathbf{X} + \rho_L \mathbf{a} \tag{11}$$

where the vector $\mathbf{a}$ is a unit vector perpendicular to the magnetic field that defines the position of the particle in relation to the guiding centre. On the other hand, the velocity of the particle can be written as [15]:

$$\mathbf{v} = v_\perp \mathbf{c} + v_\parallel \mathbf{b} \tag{12}$$

with $v_\parallel$ the parallel velocity to the magnetic field, $\mathbf{b}$=$\mathbf{B}$/B the unit vector in the magnetic field direction and $\mathbf{c}$ a unit vector in the direction of the perpendicular velocity. The vectors $\mathbf{a}$ and $\mathbf{c}$ are defined such that $\mathbf{a} = \mathbf{b} \times \mathbf{c}$ and they implicitly define the gyrophase $\xi$ [15]

$$\mathbf{a} = cos\xi \mathbf{e}_1 - sin\xi \mathbf{e}_2 \tag{13}$$

$$\mathbf{c} = -sin\xi \mathbf{e}_1 - cos\xi \mathbf{e}_2 \tag{14}$$

where $\mathbf{e}_1$ and $\mathbf{e}_2$ are two unit vectors defined such that $\mathbf{e}_1 \times \mathbf{e}_2 = \mathbf{b}$.

The Lagrangian of the guiding centre motion is described by the variables $\mathbf{X}$, $v_\parallel$, $v_\perp$ and $\xi$ and it was obtained by Littlejohn [15]:

$$\mathcal{L}_{GC} = [z\mathbf{A} + mv_\parallel \mathbf{b}].\dot{\mathbf{X}} + \frac{m}{z}\frac{mv_\perp^2}{2B}\dot{\xi} - H(v_\parallel, v_\perp, \mathbf{X}), \tag{15}$$

where $\mathbf{A}$ is the vector potential evaluated at the position of the guiding-centre and $H = mv_\parallel^2/2 + \mu B + z\Phi$ is the Hamiltonian of the system, with $\Phi$ the electric potential, also evaluated at the position of the guiding-centre.

The equations of motion for the guiding centre are then derived from the Euler-Lagrange equations (6), where the $q^i$'s are the guiding centre's variables. The equations for the guiding-centre's position and parallel velocity are [15]

$$\dot{\mathbf{X}} = \frac{1}{B_\parallel^*}\left[v_\parallel \mathbf{B}^* + \mathbf{b} \times \left(\frac{\mu}{z}\nabla B - \mathbf{E}^*\right)\right] \tag{16}$$

$$\dot{v_\parallel} = -\frac{z}{m}\frac{1}{B_\parallel^*}\mathbf{B}^*.\left(\frac{\mu}{z}\nabla B - \mathbf{E}^*\right) \tag{17}$$

where

$$\mathbf{B}^* = \mathbf{B} + \frac{m}{z} v_\parallel \nabla \times \mathbf{b}, \quad B_\parallel^* = B + \frac{m}{z} v_\parallel (\mathbf{b}.\nabla \times \mathbf{b})$$
$$\text{and} \quad \mathbf{E}^* = \mathbf{E} - \frac{m}{z} v_\parallel \frac{\partial \mathbf{b}}{\partial t}.$$

### 3.2. Constants of motion

In equilibrium, the fields are time-independent and so are the Lagrangians, therefore the energy is conserved and it is given by

$$E = \frac{1}{2} m \mathbf{v}.\mathbf{v} + z\Phi. \tag{18}$$

And for the guiding-centre approximation:

$$E_{GC} = \frac{1}{2} m v_\parallel^2 + \mu B + z\Phi. \tag{19}$$

In an axisymmetric tokamak, the equilibrium fields are also independent of the toroidal angle $\phi$, therefore another constant arises from the Lagrangians, which is the toroidal angular momentum

$$P_\phi = \frac{\partial \mathcal{L}}{\partial \dot{q}^\phi} = m v_\phi + z A_\phi. \tag{20}$$

And for the guiding-centre approximation:

$$P_{\phi_{GC}} = \frac{\partial \mathcal{L}_{GC}}{\partial \dot{q}^\phi} = -z\psi \pm m b_\phi \sqrt{\frac{2E}{m}\left(1 - \frac{\Lambda B}{B_0}\right)} \tag{21}$$

where $\psi = -A_\phi$ is the magnetic field flux, $\Lambda = \frac{\mu B_0}{E}$, $B_0$ is the magnetic field at the magnetic axis and $\mu = \frac{m v_\perp^2}{2B}$ is the magnetic moment.

In the guiding-centre approach, another constant of motion arises, the magnetic moment, $\mu$, which results from the absence of the gyrophase in the Lagrangian

$$\mu = \frac{m v_\perp^2}{2B}. \tag{22}$$

## 4. Time integration methods

To compute a particle's trajectory, one needs to integrate the equations of motion, which are a system of two vectorial ordinary differential equations (ODEs): one for the position and another for the velocity. In some simple cases, the solutions for the position and velocity can be found analytically. But when that is not possible, there are several numerical methods that can be used to find an approximation to the exact solution. Consider a first order ODE of the form

$$\frac{dy(t)}{dt} = f(y, t) \tag{23}$$

The solution $y(t)$ at a given time $t_{n+1} = (n+1)\Delta t$, where $\Delta t$ is the time-step, can be obtained from the solution at a previous time $t_n$ by a single-step method using

$$y_{n+1} = y_n + \Delta t \Phi(y_n, t_n) \tag{24}$$

where $\Phi(y_n, t_n)$ is a function of the parameters at time $t_n$ and it depends on the integration method used.

Runge-Kutta (RK) methods are a family of integration methods to solve an ODE of the type (23) [16]. One of the most popular RK methods is the classical RK of order 4 which can be written as:

$$y_{n+1} = y_n + \frac{\Delta t}{6}(k_1 + 2k_2 + 2k_3 + k_4) \tag{25}$$

with

$$k_1 = f(t_n, y_n) \tag{26}$$
$$k_2 = f\left(t_n + \frac{\Delta t}{2}, y_n + \Delta t \frac{k_1}{2}\right) \tag{27}$$
$$k_3 = f\left(t_n + \frac{\Delta t}{2}, y_n + \Delta t \frac{k_2}{2}\right) \tag{28}$$
$$k_4 = f(t_n + \Delta t, y_n + \Delta t k_3). \tag{29}$$

This method is widely used to solve differential equations and, because its numerical error is proportional to $\Delta t^4$, it is sufficiently accurate for most situations. But the global error of the RK4 method growths exponentially with time, making it unfit for simulations over long times. Besides the accumulation of error, a method such as RK4 can become computationally demanding, since, for each time-step, it is necessary to evaluate the right-hand side of each ODE four times.

### 4.1. Boris algorithm

The Boris algorithm, due to its simplicity and long-time accuracy, is widely used to solve the equations of motion of a charged particle in an electromagnetic field using cartesian coordinates, i.e., to solve the system of equations (9). This algorithm, first introduced by Boris in 1970 [17], defines a one-step method to obtain $(\mathbf{x}_{k+1}, \mathbf{v}_{k+1/2})$ from $(\mathbf{x}_k, \mathbf{v}_{k-1/2})$ [18]:

$$\mathbf{x}_{k+1} = \mathbf{x}_k + \Delta t \mathbf{v}_{k+1/2} \tag{30}$$

$$\mathbf{v}_{k+1/2} = \mathbf{v}_{k-1/2} + z\frac{\Delta t}{m}\left[\mathbf{E}_k + \frac{(\mathbf{v}_{k-1/2} + \mathbf{v}_{k+1/2})}{2} \times \mathbf{B}_k\right] \tag{31}$$

where $\Delta t = t_{k+1} - t_k$ is the time step, $t_k \equiv k\Delta t$, $\mathbf{x}_k \equiv \mathbf{x}(t = t_k)$, $\mathbf{v}_{k-1/2} \equiv \mathbf{v}(t = t_k - \Delta t/2)$, $\mathbf{v}_{k+1/2} \equiv \mathbf{v}(t = t_k + \Delta t/2)$,$\mathbf{E}_k \equiv \mathbf{E}(\mathbf{x}_k)$ and $\mathbf{B}_k \equiv \mathbf{B}(\mathbf{x}_k)$.

Due to equation (31), the algorithm looks like an implicit method. However, this equation can be expressed in a way that isolates $\mathbf{v}_{k+1/2}$, therefore making it explicit. The strategy is to separate the electric from the magnetic forces as follows: half of the electric impulse is added to the velocity, then a rotation of the velocities due to the magnetic field is applied and finally, the other half of the electric impulse is added:

$$\mathbf{v}^- = \mathbf{v}_{k-1/2} + \frac{q}{m}\frac{\Delta t}{2}\mathbf{E}_k \tag{32}$$

$$\frac{\mathbf{v}^+ - \mathbf{v}^-}{\Delta} = \frac{q}{2m}(\mathbf{v}^+ + \mathbf{v}^-) \times \mathbf{B}_k \tag{33}$$

$$\mathbf{v}_{k+1/2} = \mathbf{v}^+ + \frac{q}{m}\frac{\Delta t}{2}\mathbf{E}_k. \tag{34}$$

One major advantage of this algorithm is that it preserves energy exactly when there's no electric field, i.e.,

$\mathbf{v}_{k+1/2}.\mathbf{v}_{k+1/2} = \mathbf{v}_{k-1/2}.\mathbf{v}_{k-1/2}$. When there's an electric field, the total energy is not numerically conserved, but it has been shown that the Boris algorithm presents a bound of the total energy error. The reason for this was presented by *Qin et al* in [18], where it is shown that although the algorithm is not symplectic, it preserves phase-space volume, which is a characteristic shared with symplectic algorithms.

## 5. Implementation

To compute the particles' trajectories in tokamaks, it is necessary to have accurate representations of the magnetic and electric fields. For the purposes of this work, a tokamak equilibrium field is obtained from the code `HELENA` [19]. A particular coordinate system is also defined by the code, with a radial coordinate $s = \sqrt{\psi/\psi_b}$, where $\psi$ is the poloidal flux and $\psi_b$ its value at the plasma boundary, the angle $\chi$, defined such that $q(\chi) = B^\phi/B^\chi$, and the toroidal angle $\phi$. In addition to the equilibrium field, an electromagnetic perturbation, that will represent an Alfvén Eigenmode, is also implemented. The perturbation was obtained using the MHD code `CASTOR`, which uses the same coordinate system as `HELENA`. The data provided by the codes is defined in a discrete $(s, \chi)$ grid, therefore two-dimensional interpolations are needed to obtain the magnetic fields in the desired positions. The $(s, \chi)$ grid is regular and uniform, which allows the use of a Bi-cubic interpolator from the GSL library [20].

To simulate a particle trajectory, the equations of motion must be integrated in time. To accomplish this, it is necessary to define the initial state of the particle, which will then be evolved using an integration method that has access to the electromagnetic field that is changing the particle state. In the present work, the particles' trajectories will be computed for the two formalisms: guiding-center(GC) and full-orbit(FO).

### 5.1. Guiding-centre trajectory

The initial conditions define the state of the particle at the beginning of the simulation and are needed to solve the equations of motion, with each requiring one initial condition. In the guiding-centre approach, four initial conditions must be given: the three components of the position $\vec{x}_{GC}(s, \chi, \phi)$ and the parallel velocity $v_\parallel$, which can be obtained from the constants energy and $\Lambda$, $v_\parallel = \sqrt{\frac{2E}{m}\left(1 - \Lambda\frac{B}{B_0}\right)}$.

The equations of motion for the guiding-centre are (16) and (17) and can be solved in the `HELENA`'s coordinate system by a Runge-Kutta method.

### 5.2. Full-orbit trajectory

In the full-orbit approach, six initial conditions must now be given: the three components of the position $\vec{x}_{FO}(s, \chi, \phi)$ and the three components of the velocity $\vec{v}_{FO}(\dot{s}, \dot{\chi}, \dot{\phi})$. In order to compute trajectories that correspond to the same particle, the full-orbit initial conditions can be obtained from the guiding-center conditions:

$$\begin{cases} \vec{x}_{FO} = \vec{x}_{GC} + \rho_L \hat{a} \\ \vec{v}_{FO} = v_\parallel \vec{b} + v_\perp \hat{c} \end{cases} \tag{35}$$

with $\rho_L = \frac{m v_\perp}{qB}$, $\vec{b}$ the unit vector in the direction of the magnetic field and $v_\perp = \sqrt{\frac{2E}{m}\Lambda\frac{B}{B_0}}$. To define the unit vectors $\vec{a}$ and $\vec{c}$, an additional condition must be given: the gyrophase $\xi$. This condition allows the definition of $\vec{a}$ and $\vec{c}$

$$\begin{cases} \hat{a} = cos(\xi)\hat{e_1} - sin(\xi)\hat{e_2} \\ \hat{c} = -sin(\xi)\hat{e_1} - cos(\xi)\hat{e_2} \end{cases} \tag{36}$$

where the unit vectors $\hat{e_1}$ and $\hat{e_2}$ are defined such that they are perpendicular to the magnetic field. A contravariant unit vector can be defined as $\hat{e_1} = \{1, 0, 0\}$. Since $B^s = 0$, $\hat{e_1}$ and $\vec{b}$ are perpendicular, and then $\hat{e_2} = \vec{b} \times \hat{e_1}$.

In the coordinate system defined by `HELENA`, the metric is position dependent, therefore the equations of motion that must be used to solve the full-orbit are the most general ones in equation (7), where the indices $k, i, j, n = s, \chi, \phi$. Each seconder order ODE can be written as a system of two first order ODE's

$$\begin{cases} \frac{d}{dt}q^i = \dot{q}^i \\ \frac{d}{dt}\dot{q}^i = -g^{im}\Gamma_{mjk}\dot{q}^j\dot{q}^k + \frac{z}{m}(E^i + [\dot{\mathbf{q}} \times \mathbf{B}]^i) \end{cases} \tag{37}$$

which corresponds to six first order ODE's. This system can be solved by a classical fourth-order Runge-Kutta method.

If a Cartesian coordinate system is used, the equations of motion become simply

$$\begin{cases} \frac{d}{dt}q^i = \dot{q}^i \\ \frac{d}{dt}\dot{q}^i = \frac{z}{m}(E^i + [\dot{\mathbf{q}} \times \mathbf{B}]^i) \end{cases} \tag{38}$$

with $i = x, y, z$. This system can be solved by the Boris algorithm. To start the integration using the Boris method, it is necessary correct the initial velocity by going back a half time-step as follows:

$$\mathbf{v}_{k-1/2} \approx \mathbf{v}_k - \frac{\Delta t}{2}\frac{z}{m}(\mathbf{E}_k + \mathbf{v}_k \times \mathbf{B}_k) + \mathcal{O}(\Delta t^2) \tag{39}$$

where the subscript $k$ and $k - 1/2$ represent the quantity at a given time and at half a time step before that time, respectively. One downside of this method is that the coordinates $(s, \chi, \phi)$ that define the magnetic field cannot be used and all the necessary quantities (position, velocity, electric and magnetic field) must be transformed into cartesian coordinates at each time step.

## 6. Benchmark between integration methods

In this work, an up-down symmetric ITER-like equilibrium is used in all simulations presented. The position of the magnetic axis is $R_{mag} = 6.4$ m, the minor radius, is $a = 2.0$ m, and the magnitude of the magnetic field on the axis is $B_0 = 5.3$ T. In equilibrium, there is no electric field. In this scenario, the Larmor radius for deuterium ions is $\rho_d \approx 1.5$ mm, while for alpha particles is $\rho_\alpha \approx 3.6$ cm. Comparing these lengths with the spatial scale for the background field, which is $a \approx 2$ m, both of them are very small: $\rho_d, \rho_\alpha \ll a$. Therefore, the particles' trajectories should be well approximated by the guiding-centre description. To compute the full-orbit, the Boris

algorithm and a $4^{th}$ order RK method will be compared in order to understand which is the most suitable for full-orbit simulations.

First, the trajectory of a passing 3.5 MeV $\alpha$-particle is computed using the three possible methods: guiding-centre, full-orbit using the RK4 method and full-orbit using the Boris algorithm. Besides an energy of 3.5 MeV, the initial conditions used were $\Lambda = 0.3$, position of the guiding-centre $s = 0.5, \chi = 0.0, \phi = 0.0$ and, for the full-orbit simulations, the gyrophase was set to $\xi = \pi/2$. Figure 3 represents the trajectories obtained by the three methods. Both RK4 and Boris give the same full-orbit trajectory and the guiding-centre produces its average, as expected.

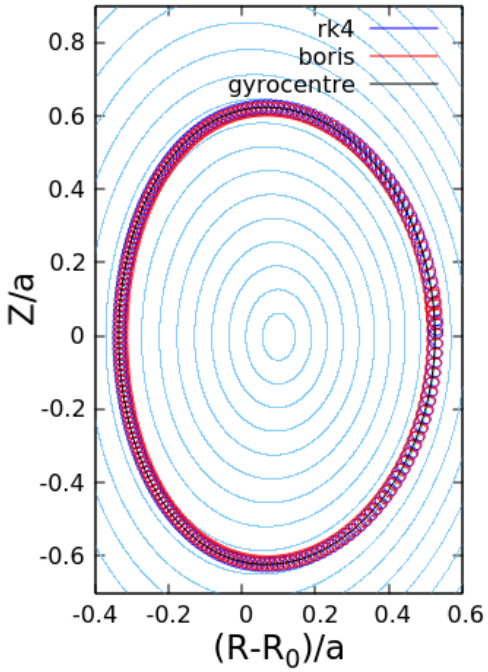


Figure 3: Orbit of a 3.5MeV passing particle computed using the RK4 method and the Boris algorithm for the full-orbit and the guiding-centre.

The orbit integration was performed using a time-step adequate to the integration method used. With the GC approach, the time-step used was $4.00 \times 10^{-8}$ s, while for the FO integration the time-step was set to be $T/40$, where $T = 2\pi/\Omega$ is the period of one gyration, which gives $\Delta t = 6.94 \times 10^{-10}$ s, about 60 times shorter than the time-step used in GC integration.

A major difference between using RK4 and the Boris method is the conservation of energy. While for RK4 the energy difference relative to the initial energy is about $6.4 \times 10^{-4}$, for Boris is of order $10^{-14}$. This was expected since the Boris algorithm does conserve energy exactly, so the only error is the one due to the round-off of the machine. The smaller energy error associated with the Boris algorithm, also allows it to have a larger time-step without increasing the error in energy. Due to its construction, the energy error of the Boris algorithm is of the order $10^{-14}$ independently of the time-step, while with RK4 the error increases with increasing time-step.

One of the main advantages of the Boris algorithm against the RK4 integration method resides in the fact that the first conserves energy exactly and therefore gives the right trajectory even after a long simulation time [18]. To test that, the trajectories of the same particle from the previous case were computed for ten poloidal orbits. The trajectories of the last turn are presented in figure 4 and the energy evolution for the two FO methods is represented in figure 5.

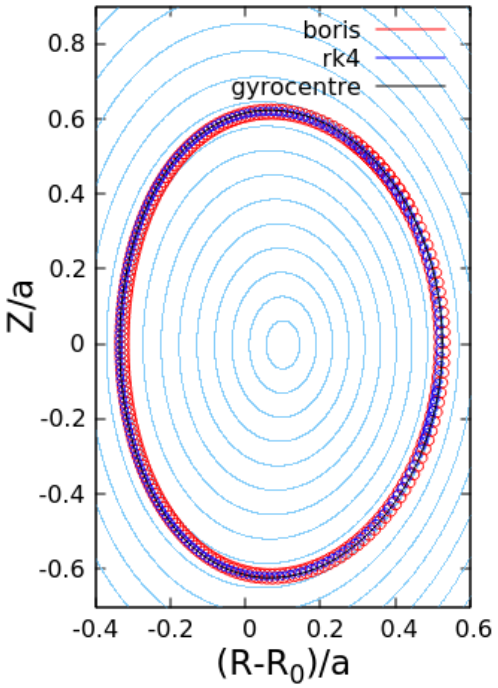


Figure 4: Orbit of a 3.5MeV passing particle computed using the RK4 method and the Boris algorithm for the full-orbit and the guiding-centre after 10 turns.

It is clear from the figure that after 10 turns the RK4 method no longer gives the correct orbit, as the Larmor radius is much shorter than in the first turn. From figure 5, the energy decreases by 42.7%, explaining the smaller Larmor radius in the last turn. On the other hand, the Boris method holds up the right trajectory, which can be understood due to the conservation of energy verified with the Boris algorithm.

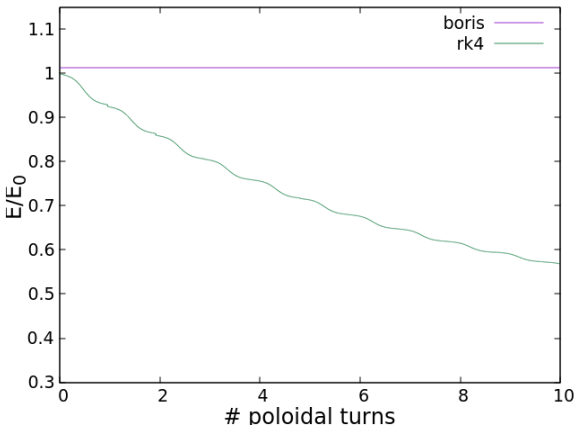


Figure 5: Energy evolution for the Boris algorithm and the RK4 method.

### 6.1. Computational time

Full-orbit computations need a time-step about 60 times smaller than the one used for the guiding-centre. Therefore, the computational effort of the integration method is very important, especially when the simulation needs to run for a long time. For both full-orbit methods, the simulation was performed, using the same time-step, for different simulation times and the computational times were determined. The results are presented in figure 6.

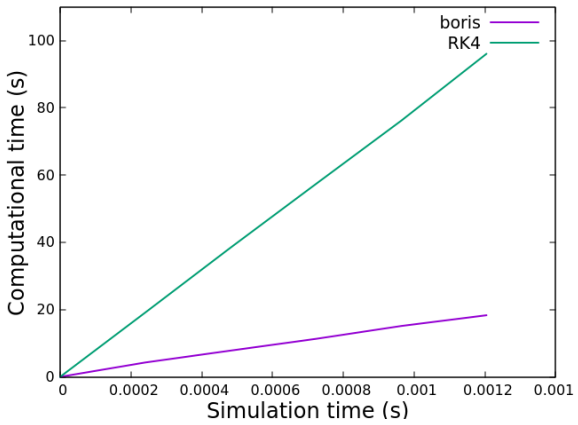


Figure 6: Computational times for the RK4 and Boris methods.

The Boris algorithm, although needing to deal with coordinate transformation, is much faster than the RK4 method, by approximately 5 times. This difference in computational time and exact energy conservation makes the Boris algorithm preferred to the RK4 method when simulating the full-orbit of charged particles in electromagnetic fields. Therefore, in the following sections, the Boris algorithm was used for all full-orbit simulations presented.

## 7. Alfvén Eigenmodes in ITER

This section is dedicated to studying the influence of Alfvén Eigenmodes in the dynamics of $\alpha$-particles in an ITER scenario. Two different modes are used in order to compare the results given by the guiding-centre and the full-orbit approaches, testing the validity of the guiding-centre approximation.

The modes used take the form $\mathbf{A}(\mathbf{x})e^{-i(\mathbf{k}.\mathbf{x}+\omega t)}$, where $\mathbf{A}(\mathbf{x})$ gives the amplitude of the mode, $\mathbf{x}$ is the position, $\mathbf{k}$ is the wave vector and $\omega$ is the perturbation frequency. The covariant components of the wave vector can be expressed in terms of the mode numbers $m$ and $n$: $k_\theta = m$ and $k_\phi = n$ and therefore, the perturbation can be written as $\mathbf{A}(s)e^{-i(n\phi - m\theta + \omega t)}$ [5]. The guiding-centre approximation is valid if the wavelength of the perturbation is much larger than the Larmor radius so that within the Larmor radius the perturbation does not change significantly. The Larmor radius is measured in the perpendicular direction, therefore it needs to be compared only with the perpendicular component of the wave vector, $k_\perp$. Consequently, the condition to be verified is

$$k_\perp \rho_L \ll 1. \tag{40}$$

### 7.1. Particle-wave energy exchange

An electromagnetic wave is associated with an electric field $\mathbf{E}$ and a magnetic field $\mathbf{B}$. A particle with charge $q$ and velocity $\mathbf{v}$ moving in presence of a wave interacts with it via a force $\mathbf{F} = q(\mathbf{E} + \mathbf{v} \times \mathbf{B})$. An exchange of energy between a charged particle and a wave only takes place if the force $\mathbf{F}$ driving the particle's motion has a component parallel to the particle's velocity $\mathbf{v}$ [13] since the work is given by

$$W = \int \mathbf{F}.d\mathbf{s} = \int \mathbf{F}.\mathbf{v}dt. \tag{41}$$

Moreover, the energy transfer between a particle and an electromagnetic wave can only occur if the value of $\mathbf{v}.\mathbf{E}$ is non-zero, since $(\mathbf{v} \times \mathbf{B}).\mathbf{v} = 0$. The energy exchange in a time step, i.e. between $t_k$ and $t_{k+1}$, is the transfer of energy due to the work given by

$$W_k = \int_{t_k}^{t_{k+1}} \mathbf{F}(\mathbf{x}).d\mathbf{s} = q\int_{t_k}^{t_{k+1}} \mathbf{E}[\mathbf{x}(t)].\mathbf{v}(t)dt. \tag{42}$$

When using the guiding-centre, the work is calculated considering $\mathbf{x}$ as the guiding-centre position, $\mathbf{x}_{GC}$, and $\mathbf{v}$ as the derivative of guiding-centre positions, i.e., $\mathbf{v}_{GC}(t) = \frac{d\mathbf{x}_{GC}(t)}{dt}$. The work in one time-step is calculated using

$$W_{k_{GC}} \approx q\Delta t \mathbf{v}_k.\mathbf{E}_{k_{GC}} \tag{43}$$

with $\Delta t = t_{k+1} - t_k$. In the full-orbit approach, the Boris algorithm is used, where positions and velocities are considered at different times. To calculate the work, Taylor's expansions are taken around $t_{k+1/2}$ for the velocity and around $t_k$ for the electric field. With these approximations, the work $W_k$ is approximated by

$$W_k \approx q\Delta t \mathbf{E}_k.\mathbf{v}_{k+1/2} + q\frac{\Delta t}{2}(\mathbf{E}_{k+1} - \mathbf{E}_k).\mathbf{v}_{k+1/2}. \tag{44}$$

In both cases, for a given time $t$, the total work is simply the sum of the work in all time-steps

$$W(t) = \sum_{k=0}^{k=t/\Delta t} W_k. \tag{45}$$

### 7.2. Resonant $\alpha$-particle with n=30 mode

The guiding-centre initial conditions of an $\alpha$-particle that leads to a resonant interaction with the mode $n = 30$ were obtained with the code `CASTOR-K` [21]: $E = 3.362$ MeV, $\Lambda = 0.1725$ and $P_\phi = 6.66156$ eV.s. The correspondent initial position for these conditions is $s = 0.3676, \chi = 0, \phi = 0$. For this particle, the Larmor radius is $\rho_\alpha \approx 0.021$ m and the perpendicular wave vector of the $n = 30$ mode is $k_\perp \approx 30.9$. Therefore $\rho_\alpha k_\perp \approx 0.64$, not satisfyng condition (40) for the validity of the guiding-centre.

Using the initial conditions found, the trajectory was computed using the two approaches (GC and FO) for the equilibrium field and for the equilibrium field with the mode superimposed. For the full-orbit, one also needs a value for the gyrophase to perform the integration, so it was chosen to be $\xi = 7\pi/4$. In figure 7 the orbits computed

with the guiding-centre and with the full-orbit for both electromagnetic fields (equilibrium and perturbed ones) are represented.

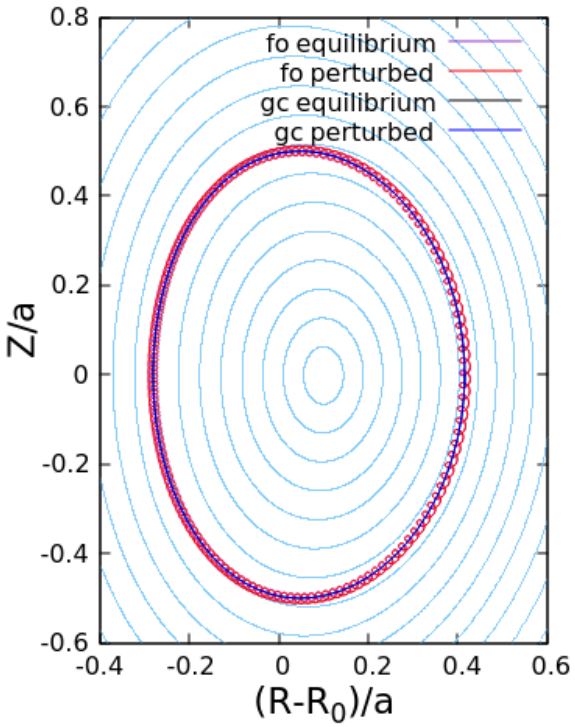


Figure 7: Orbit calculated with the guiding-centre and the Boris algorithm in equilibrium and with the n=30 mode.

From the orbit computations, there are, apparently, no differences between equilibrium and perturbed electromagnetic field nor between the orbit computed with the guiding-centre and with the full-orbit. The fact that there are no visible differences in the orbits due to the perturbation can be understood from the low magnitude of the perturbed magnetic field, which is at its maximum $3\times10^{-4}$ of the magnitude of the equilibrium field on axis, therefore not violating the conditions (10). The GC and FO orbits are in agreement, but the values for the energy exchange are quite different. The work computed for the first 10 poloidal turns for both approaches is represented in figure 8.

From the figure, the works calculated using GC and FO are very different. The average of the work is overestimated by the guiding-centre in about 400%. This difference is quite significant, which raises questions about the validity of using the GC approach. An attempt was made to correct $\mathbf{E}$ and $\mathbf{v}$ to include finite Larmor radius effects, so that the guiding-centre's equations of motion can still be used. The corrections tried to improve the work calculated with GC are now described.

First, at each time-step $\Delta t$, a circle of radius $\rho_L(\mathbf{X}) = \frac{mv_\perp(\mathbf{X})}{qB(\mathbf{X})}$ can be defined by $N$ points around the position of the GC, which is assumed to have a uniform motion in the parallel direction at each point. The GC position is advanced for each point, considering it corresponds to a slice of time $\frac{\Delta t}{N}$

$$\mathbf{X}_{i+1} = \mathbf{X}_i + \frac{(i+1)\Delta t}{N} v_\parallel \hat{b} \tag{46}$$

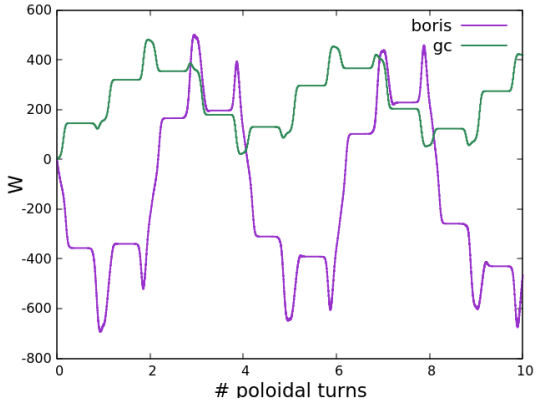


Figure 8: Evolution in time of the work between the particle and the wave computed with the guiding-centre and with the Boris algorithm.

with $i = 1, ..., N$, and the circle is defined by the points

$$\mathbf{x}_i = \mathbf{X}_i + \rho_L(\mathbf{X}_i)\hat{\rho_{L_i}}. \tag{47}$$

with

$$\hat{\rho_{L_i}} = (cos\alpha_i \hat{a} + sin\alpha_i \hat{c}). \tag{48}$$

The initial angle $\alpha$ corresponds to the initial gyrophase given in the FO, $\alpha_1 = \xi$, and is evolved at each point as $\alpha_i = \alpha_{i-1} + n \times 2\pi \frac{i+1}{N}$, where $i = 2, 3, ..., N$ is the iteration and $n$ is the number of gyrations per time step $n = \Delta t/T$, where the period is $T = 2\pi/\Omega$.

Secondly, the gyration velocity ignored in GC at each point of the circle can be retrieved

$$\mathbf{v}_{gyr_i} = v_{\perp_i}(\hat{b} \times \hat{\rho_L}) \tag{49}$$

with $v_{\perp_i}(\mathbf{X}_i) = \sqrt{E\Lambda \frac{B(\mathbf{X}_i)}{B_0}}$, and can then be added to the velocity of the guiding-centre.

Lastly, one can compute the work considering the position and velocity corrections

$$W_{GC'} = q \sum_{k=0}^{k=t/\Delta t} \frac{\Delta t}{N} \left( \sum_{i=1}^{N} \mathbf{E}(\mathbf{x}_{k_i}).(\mathbf{v}_{GC_k} + \mathbf{v}_{gyr_{k_i}}) \right). \tag{50}$$

The work computed for the first 10 poloidal turns for the FO approach and for the GC approach with corrections to the work is represented in figure 9.

From figure 9, the function of the work with corrections is in much better agreement with the work computed with the full-orbit than the work computed with the GC in figure 8. Now, the difference in the averages is about 7.69%.

To test the computational efficiency of adding these corrections, a simulation for 100 poloidal turns was performed. The guiding-centre simulation takes about $40.5s$. When adding the corrections, and taking $N = 20$, this times increases to $121.3s$, which is three times the guiding-centre computational time. On the other hand, the Boris algorithm takes $85.5s$, which is twice the guiding-centre computational time, but it is quicker than computing corrections to the guiding-centre work at each time step. Taking this into consideration, computing the full-orbit with the Boris algorithm is preferable to computing the guiding-centre and add corrections to the work.

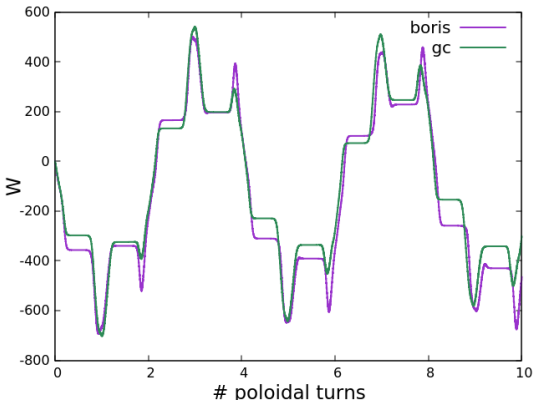


Figure 9: Evolution in time of the work between the particle and the wave for the guiding-centre with corrections and for the Boris algorithm.

### 7.3. Resonant $\alpha$-particles with n=12 mode

In order to study the interaction between an $\alpha$-particle and a mode with different values of $k_\perp \rho_\alpha$, a $n = 12$ mode was used. For six different $\Lambda$'s between 0.01 and 0.7, the initial conditions that lead to a resonant interaction were obtained using `CASTOR-K`. The orbits of these passing particles show a good agreement between GC and FO. In figure 10, the ratio $W_{FO}/W_{GC}$ is represented as a function of $k_\perp \rho_\alpha$. With increasing $k_\perp \rho_\alpha$, the computed work with the GC approach deviates from the one computed with the FO approach, which was already expected. The Larmor radius increases with increasing $k_\perp \rho_\alpha$, which means that the particles deviate further away from the guiding-centre position and a larger difference in the electric field is expected.

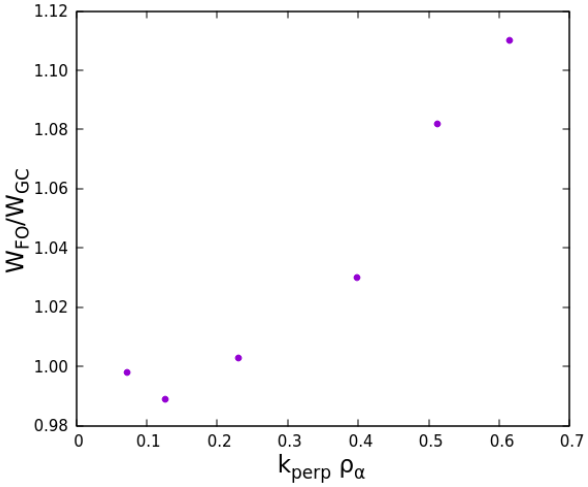


Figure 10: Ratio $W_{FO}/W_{GC}$ as a function of $k_\perp \rho_\alpha$.

### 7.4. Trapped particles

Until now, only passing particles were considered. A trapped particle with initial conditions $E = 1317keV$, $\Lambda = 1.1$ and $P_\phi = 10.811(eV.s)$ is now analyzed and its orbit is represented in figure 11.

The trajectories for this trapped particle interacting with the $n = 12$ mode are different in both approaches, which results in different values for the work,

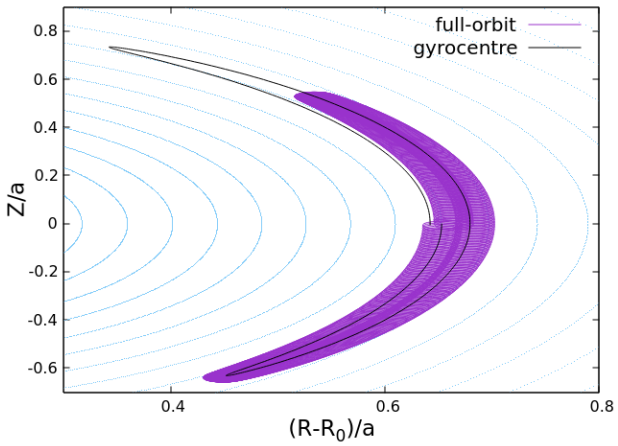


Figure 11: Orbit of an $\alpha$-particle with $\Lambda = 1.1$ computed with the guiding-centre and full-orbit approaches.

$W_{FO}/W_{GC} \approx -2.6$. The energy exchange given by both approaches are different, therefore the energy of the particle is also different, which explains the tips of the trapped particles occurring at different positions seen in figure 11.

## 8. Conclusions

The first achievement of this work was the implementation and benchmark of two different time integration methods to solve the equations of full-orbit motion of charged particles in tokamaks' electromagnetic fields: the 4-th order Runge-Kutta and the Boris algorithms. The first difference between them is that the first one can solve the equations for any coordinate system, while the second is only able to solve the equations of motion in a cartesian coordinate system, which demands a transformation of coordinates to be performed at each time step. An ITER-like magnetic equilibrium field, obtained from the code `HELENA`, was used to test the integration methods in relation to their conservation properties of the constants of motion and computational performance. The Boris algorithm proved to conserve energy exactly, while for the Runge-Kutta method, the error in energy was seen to increase exponentially. In relation to their computational efficiency, the Boris algorithm is approximately five times faster than the Runge-Kutta method, despite the coordinate transformations required by the former. Therefore, the Boris algorithm was chosen to carry out the subsequent full-orbit simulations.

In the second part of this work, the validity of the guiding-centre approximation was tested for the interaction of resonant $\alpha$-particles with Alfvén Eigenmodes in ITER. For an $\alpha$-particle in resonance with a mode $n = 30$, the value of $k_\perp \rho_\alpha$ is close to 1, which does not satisfy the validity condition $k_\perp \rho_\alpha \ll 1$ for the guiding-centre approximation. In this case, the orbits calculated with the guiding-centre showed a good agreement with the full-orbit. However, the same agreement was not found for the energy exchange. Based on the connection between the variables of the guiding-centre and full-orbit, some correction to the work calculated with the guiding-centre were attempted. These corrections decreased significantly the difference between the work calculated with both ap-

proaches. However, the computational effort associated with the corrections needed is too heavy and costly, while computing the full-orbit with the Boris algorithm was found to be less demanding.

Because the values of $k_\perp \rho_\alpha$ are always close to 1 for the $n = 30$ mode, a mode with $n = 12$ was used to test the validity of the guiding-centre for a variety of values of $k_\perp \rho_\alpha$. The orbits of passing particles were well approximated by the guiding-centre. The energy exchange calculated with both approaches showed a good agreement for lower values of $k_\perp \rho_\alpha$ and the difference increases for higher values, as expected. For trapped particles, the orbits computed with both approaches do not agree. The energy exchange is different, which directly implies that the energy of the particles is different and therefore the tips of the trapped particles occur at different positions.

In summary, when following charged particles in fusion plasmas, the Boris algorithm performs better than the RK4 method. Moreover, RK4 should be avoided in simulations for long times. Regarding the guiding-centre approximation, when dealing with the ITER equilibrium field, it holds up. But, when imposing an Alfvén Eigenmode, this approximation should be used with care: for particles with values of $k_\perp \rho_L \sim 1$ the energy exchange calculated is not correct and for trapped particles, guiding-centre orbits do not match full-orbit ones. In those two cases, the guiding-centre approximation should be discarded and the full-orbit approach should be used.

**References**


[1] J. Wesson. *Tokamaks*. Oxford University Press, 2004.

[2] International Atomic Energy Agency. *Summary of the ITER Final Design Report*. Number 22 in ITER EDA Documentation Series. Vienna, 2001.

[3] Simon Pinches et al. The role of energetic particles in fusion plasmas. *Plasma Physics and Controlled Fusion*, 46:B187, 12 2004.

[4] S Pinches et al. Energetic ions in ITER plasmas. *Physics of Plasmas*, 22(2):21807, 2015.

[5] P Rodrigues et al. Systematic linear-stability assessment of Alfvén eigenmodes in the presence of fusion alpha-particles for ITER-like equilibria. *Nuclear Fusion*, 55(8), 2015.

[6] M. Fitzgerald et al. Predictive nonlinear studies of TAE-induced alpha-particle transport in the Q = 10 ITER baseline scenario. *Nuclear Fusion*, 56(11), 2016.

[7] M. Schneller, Ph Lauber, and S. Briguglio. Nonlinear energetic particle transport in the presence of multiple Alfvénic waves in ITER. *Plasma Physics and Controlled Fusion*, 58(1), 2015.

[8] Ph Lauber. Local and global kinetic stability analysis of Alfvén eigenmodes in the 15 MA ITER scenario. *Plasma Physics and Controlled Fusion*, 57(5):54011, 2015.

[9] E Hirvijoki et al. ASCOT: Solving the kinetic equation of minority particle species in tokamak plasmas. *Computer Physics Communications*, 185(4):1310–1321, 2014.

[10] G J Kramer et al. A description of the full-particle-orbit-following SPIRAL code for simulating fast-ion experiments in tokamaks. *Plasma Physics and Controlled Fusion*, 55(2), 2013.

[11] RJ Akers et al. Gpgpu monte carlo calculation of gyro-phase resolved fast ion and n-state resolved neutral deuterium distributions. In *Proc. 39th EPS Conference on Plasma Physics*, page P5, 2012.

[12] C. Sommariva et al. Test particles dynamics in the JOREK 3d non-linear MHD code and application to electron transport in a disruption simulation. *Nuclear Fusion*, 58(1):016043, 2017.

[13] W Heidbrink. Basic physics of Alfvén instabilities driven by energetic particles in toroidally confined plasmas. *Physics of Plasmas*, 15(5), 2008.

[14] A Fasoli et al. Chapter 5: Physics of energetic ions. *Nuclear Fusion*, 47(6):S264, 2007.

[15] Robert G Littlejohn. Variational principles of guiding centre motion. *Journal of Plasma Physics*, 29(01):111, 1983.

[16] J.C. Butcher. *Numerical Methods for Ordinary Differential Equations*. Wiley, 2003.

[17] J P Boris. Relativistic plasma simulation-optimization of a hybrid code. *Proceeding of Fourth Conference on Numerical Simulations of Plasmas*, 1970.

[18] Hong Qin et al. Why is Boris algorithm so good? *Physics of Plasmas*, 20(8):084503, 2013.

[19] G. Huysmans, J.P. Goedbloed, and W. Kerner. Isoparametric bicubic hermite elements for solution of the grad-shafranov equation. *International Journal of Modern Physics C*, 02(01):371–376, 1991.

[20] Brian Gough. *GNU Scientific Library Reference Manual - Third Edition*. Network Theory Ltd., 3rd edition, 2009.

[21] Duarte Borba and Wolfgang Kerner. Castor-k: Stability analysis of alfvén eigenmodes in the presence of energetic ions in tokamaks. *Journal of Computational Physics*, 153(1):101 – 138, 1999.